Designing necks and wrinkles in inflated auxetic membranes

International Journal of Mechanical Sciences 268 (2024) 109031

Contents lists available at ScienceDirect

International Journal of Mechanical Sciences

journal homepage: www.elsevier.com/locate/ijmecsci

Designing necks and wrinkles in inflated auxetic membranes ☆

Sairam Pamulaparthi Venkata [a], Valentina Balbi [a], Michel Destrade [a,b], Giuseppe Zurlo [a,*]

[a] School of Mathematical and Statistical Sciences, University of Galway, University Road, Galway, H91 TK33, Ireland
[b] Key Laboratory of Soft Machines and Smart Devices of Zhejiang Province and Department of Engineering Mechanics, Zhejiang University, Hangzhou 310027, People's Republic of China

ARTICLE INFO

Keywords:
Auxetic membranes
Functionally graded materials
Hyperelasticity
Tension field theory
Wrinkling
Necking

ABSTRACT

This article presents the potentiality of inflatable, functionally-graded auxetic membranes to produce wrinkles and necks. We obtain elastic instabilities at desired locations in axisymmetric membranes and with prescribed patterns in square membranes. First, we use an analytical approach to obtain a series of universal results providing insights into the formation of wrinkles and necks in inflated, axisymmetric membranes. For example, we prove analytically that necks and wrinkles may never overlap in pressurized, axially symmetric membranes. Second, we implement the relaxed strain energy of tension field theory into a Finite Element solver (COMSOL). By tuning spatial inhomogeneities of the material moduli, we corroborate our universal results, describe the onset of wrinkling in an averaged way, and also generate non-trivial instabilities at desired locations. This study on membranes with morphing or corrugation on demand has potential applications in Braille reading and haptics.

1. Introduction

Artificially designed materials with negative Poisson's ratio thicken when stretched, in contrast to classical elastic materials, which become thinner in the directions lateral to an applied loading direction. These so-called auxetic materials have been studied in several fields, including ferromagnetics [1], crystal elasticity [2], foam structures [3], microporous materials [4], and composites [5].

Theoretically, for isotropic materials which satisfy the pointwise energy stability criterion, the Poisson ratio can take values between −1 and 0.5 for 3D solids [6,7]. For 2D solids such as membranes, the allowable Poisson's ratio value lies between −1 and 1 [8]. In contrast, Poisson's ratio for anisotropic structures has no bounds [9], which is why some biological tissues exhibit auxeticity [10–12].

Auxetic materials can be fabricated using additive manufacturing techniques, such as powder bed fusion [13,14] or subtractive manufacturing techniques, such as laser cutting for thin structures [15,16]. With the rapid advancement in additive manufacturing techniques, even complex auxetic structures can be produced at large scales in a short time. With a careful design of voids or holes at the micro-scale, auxetic properties can be obtained at the continuum level [17,18]. Recently, solution electrospinning has been used to produce auxetic biomembranes [19].

These structures have a wide range of applications, from superhydrophobic materials, with unique wetting properties [24], to soft robots with compliant actuators [25] or compliant grippers [26], to biomedical applications, with auxetic stents [27], dynamic organ patches [23], or skin grafts [28]. Fig. 1 displays examples of recent applications.

Due to their thin-walled, lightweight, and impressive tensile properties, nonlinear elastic membranes play a prominent role in many fields such as automobile, aerospace, civil and biomedical engineering [29–31]. However, thin membranes lose their mechanical stability under in-plane compressive stresses due to negligible bending rigidity, leading to interesting behaviors [7,32,33]. Inflatable membranes under large elastic deformations experience various kinds of bifurcation phenomena such as limit-point (snap-through), wrinkling, and necking instabilities. Some of the most common and significant applications of inflatable auxetic materials can be seen in stent deployment for angioplasty [34], in morphing structures [35], and for smart biomaterials [36].

Over the past several decades, there has been extensive research on finite inflation of incompressible circular membranes. Early experimental works by Flint and Naunton [37], Treloar [38], and Rivlin and Saunders [39] present a detailed analysis of the deformation shape and strain distributions over the surface of inflated incompressible isotropic balloons. Adkins and Rivlin [40] studied theoretically pressurized circular and spherical thin shells using incompressible neo-Hookean and

☆ This research project funded by the XS-META ITN: Marie Skłodowska-Curie European Actions (Grant Agreement No. 956401).
* Corresponding author.
E-mail addresses: S.PamulaparthiVenkata1@universityofgalway.ie (S. Pamulaparthi Venkata), vbalbi@universityofgalway.ie (V. Balbi), michel.destrade@universityofgalway.ie (M. Destrade), giuseppe.zurlo@universityofgalway.ie (G. Zurlo).

https://doi.org/10.1016/j.ijmecsci.2024.109031
Received 18 August 2023; Received in revised form 22 December 2023; Accepted 9 January 2024
Available online 13 January 2024

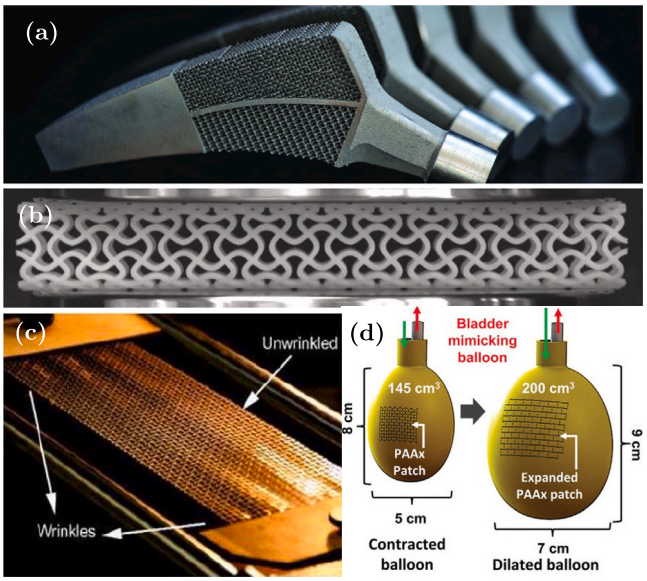

Fig. 1. Examples of applications and behaviors for auxetic materials. (a) Hip implants can be designed to include regions with a negative Poisson ratio to minimize retraction from the bone under biomechanical loading [20]. (b) Auxetic tubular lattice stents exhibit increased ductility compared to conventional diamond tubular lattices [21]. (c) Auxetic thin membranes under tension wrinkle in the neighborhood of clamps, in contrast to conventional membranes, which wrinkle in their central region [22]. (d) Auxetic patches glued onto balloon membranes can undergo larger deformations than conventional patches, a property which can help with the healing of puncture wounds to the bladder for example [23].

Mooney–Rivlin strain energy functions, to obtain the relationship between inflating pressure, extension ratio, and radius of curvature near the pole. The book by Green and Adkins [41] covers the mathematical theory of finite strain deformations in nonlinear membranes extensively for both isotropic and anisotropic materials. More recent experimental works include that by Machado et al. [42], who proposed a method to determine curvatures and membrane stresses using an axisymmetric bulge test for isotropic circular membranes and a three-dimensional digital image correlation technique.

Finite element analysis (FEA) is very useful in understanding the behavior of complex geometries and loading conditions. Many researchers have developed numerical methods based on FEA to study finite inflation in nonlinear membranes using different material models and for different geometries. For example, see the works on axisymmetric membranes by Oden and Sato [43], Wriggers and Taylor [44], Gruttmann and Taylor [45], Jiang and Haddow [46], Rumpel et al. [47], Eriksson and Nordmark [48], and Selvadurai [49], on rectangular membranes using finite difference iterative scheme by Yang and Lu [50], and on rectangular membranes using FEA by Adler and Mikulas [51], Lee and Youn [52], Barsotti and Ligarò [53], Chen et al. [54], and Li et al. [55,56].

Analytical solutions associated with the finite inflation of nonlinear membranes are scarce in the literature due to strong material and geometrical nonlinearities. However, analytical solutions play an important role in providing simplified and direct solutions to predict the mechanical behavior of inflated membranes. With an assumption of linear elastic constitutive behavior and spherical deformation shape for a pressurized incompressible isotropic circular membrane, Fichter [57] provided closed-form analytical solutions for small deformations, later extended by Coelho et al. [58] for finite strains. Relaxing the constraint of linear elastic material behavior but still assuming the spherical deformation shape of the membrane, Yuan et al. [59], Foster [60], and Yang et al. [61] derived analytical solutions for pre-stretched circular membranes under inflation using different incompressible hyperelastic material models. Dropping the hypothesis of spherical deformation shape and considering compressibility, pressure-deflection formulas for inflated isotropic circular membranes with compressible Mooney–Rivlin model are provided by Pelliciari et al. [62] without pre-stretch, by Sirotti et al. [63] with pre-stretch, and by Pelliciari and Tarantino [64] for anisotropic pressurized graphene membranes without prestretch.

Many of the above-mentioned works dealt with limit-point instability in inflatable circular membranes, but little attention has been drawn in the past to the study of wrinkling and necking instabilities for functionally-graded inflatable auxetic circular membranes under mechanical loads.

Several theories exist in the literature for studying wrinkles in nonlinear elastic membranes. For example, the theory of incremental deformations [65,66], the Föppl–von Kármán theory of plates [67,68], the reduced-order finite element membrane theory [69], the numerical bifurcation-continuation analysis [70], and an algorithm coupling the Asymptotic Numerical Method and the Chebyshev spectral collocation approach [71]. Although these advanced and refined models provide comprehensive details on the wavelength and amplitude of wrinkles, they are computationally expensive to implement.

That is because the characteristic length scale of wrinkles is typically much smaller than that of the structure and, to accurately predict wavelength and amplitude, the mesh size in finite element simulations must be much smaller than the wrinkle size [72]. Additionally, the wavelength of wrinkles decreases with the thickness of the membrane, resulting in high computational costs when shell elements are employed for simulations of large-scale membrane geometries [73]. Hence Pagitz and Pellegrino [74] mention that current scientific balloons have a diameter of 80 m and a thickness of 0.04 mm, requiring 10^{11} degrees of freedom using shell elements to accurately model the instability behavior of the pressurized balloons.

In this study, we focus on determining the average deformation in the wrinkled region along with finding the location and orientation of wrinkles, but not their amplitude and wavelength. Therefore, we employ tension field theory, originally proposed by Wagner [75] and Reissner [76]. Tension field theory has the advantage of being computationally viable and mathematically elegant [72–74]. According to tension field theory, membranes are assumed to have zero out-of-plane bending stiffness and cannot sustain in-plane compressive stresses. In the 1980s, in order to account for compressive stresses, Pipkin [77] extended the theory by introducing the concept of "relaxed strain energy function", see also Pipkin [78], Steigmann and Pipkin [79], Steigmann [80], and Pipkin [81]. Relaxed models have been used to study wrinkles in anisotropic membranes [82], electroactive elastomeric membranes [83–87], pressurized magnetoelastic circular membranes [88], and inflatable isotropic membranes under uniform pressure load [89–91].

Alongside wrinkling, necking is another interesting bifurcation phenomenon observed in nonlinear membranes, although less explored in hyperelastic isotropic circular membranes. Chaudhuri and DasGupta [92] found negative Gaussian curvature and circumferential wrinkling at the fixed rim of the hyperelastic isotropic circular membrane under inflation. Necking in pressurized elasto-plastic spherical membranes has been investigated by Needleman [93] and in pressurized elasto-plastic circular membranes by Chater and Neale [94]. However, a study on necking and multi-layered bubbling phenomenon in pressurized functionally-graded hyperelastic isotropic auxetic circular membranes is still missing in the literature.

In this work, as a proof-of-a-concept, we study the effect of varying material properties such as the Young modulus and the Poisson ratio on limit-point instabilities (snap-through), necking, and wrinkling in pressurized isotropic auxetic membranes (circular and square geometries). Through molecular dynamics simulations, Ulissi et al. [95] have shown that it is, in principle, possible to tune the mechanical properties of auxetic membranes. Here use the Blatz–Ko strain energy function to model the membrane's hyperelastic mechanical behavior. We study the effect of pre-stretches on wrinkling instabilities in auxetic circular

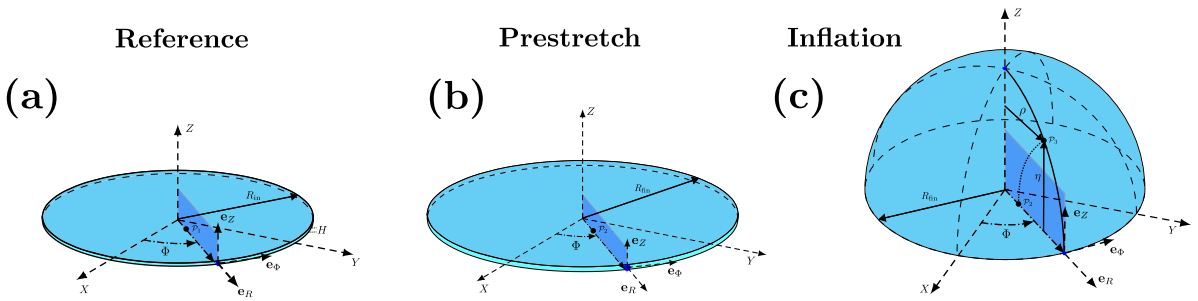

Fig. 2. Deformation profiles of the axisymmetric auxetic circular membrane. (a): Circular membrane with initial radius of R_{in} and thickness H. (b): Deformed profile of the circular membrane under radial pre-stretch with the radius R_{fin}. Note that the thickness of the membrane is increased with the in-plane stretching due to auxeticity. (c): Deformed profile of the inflated circular membrane subjected to uniform pressure P and fixed on its circumferential boundary. Point $\mathcal{P}_1$ in the undeformed configuration is displaced to the positions $\mathcal{P}_2$ and $\mathcal{P}_3$ with pre-stretch and inflation, respectively. A point in the final configuration has coordinates (ρ, Φ, η), where ρ is radial position and η is the vertical deflection.

membranes. For the onset of limit-point instabilities, we investigate the effect of pre-stretches and material parameters for circular geometries.

Finally, we show how to obtain wrinkling patterns in specific membrane areas by tuning the spatial distribution of Young's modulus and Poisson's ratio, both for square and circular membranes.

The paper is organized as follows. In Section 2, we introduce the problems of interest and the constitutive equations, and we derive the kinematics of the deformation. We also briefly summarize the main features of the relaxed strain energy functional based on tension field theory to derive the membrane stresses. Finally, we write down the equilibrium conditions along with the applied boundary conditions. In Section 3, with the help of membrane theory, we derive the equations linking curvatures and principal stresses, which are necessary for wrinkling and necking in the circular membrane. We establish several universal insights, valid for all hyperelastic isotropic membranes. These include the results that regions of necking and wrinkling cannot overlap, and that necking and wrinkling cannot occur in the center of an inflated circular membrane.

In Section 4, we compare the results of our finite element simulations in COMSOL [96] with the universal predictions of Section 3. Conclusions and limitations of the current work, along with possible directions for future works are detailed in Section 5. These include some preliminary results on square membranes which can be inflated to exhibit a desired wrinkling pattern. These results could be used in applications involving haptics.

2. Membrane deformations, energy and stress

In this work, we describe the behavior of inflated elastic membranes that are rotationally symmetric about an axis. In the so-called "membrane approximation", the membrane thickness is small in comparison to its diameter and bending effects are neglected. In this approximation, the 3D deformation is deduced from the 2D deformation of the membrane mid-surface.

We consider a circular membrane with radius R_{in} and we use a cylindrical coordinate system to represent the kinematics of the deformation. We identify the position of a point on the mid-surface of the membrane in its undeformed configuration with $\mathcal{P}_1\,(R, \Phi, 0)$. As the membrane is radially stretched axisymmetrically, the point $\mathcal{P}_1$ moves to position $\mathcal{P}_2\,(\rho_0, \Phi, 0)$ in the membrane with radius R_{fin}. Upon axisymmetric inflation of the pre-stretched membrane (with a fixed circumference) under a uniform pressure P from the side $Z = 0^-$, the membrane bulges out of the plane towards $Z = 0^+$, and the point $\mathcal{P}_2$ is displaced to position $\mathcal{P}_3\,(\rho(R), \Phi, \eta(R))$. Here, $\rho(R)$ and $\eta(R)$ represent the radial and transverse deflections of the point $\mathcal{P}_1$ in the final configuration, respectively, as shown in Fig. 2.

The in-plane stretches of the 2D membrane are calculated as

$$\lambda_1 = \sqrt{\left(\frac{\mathrm{d}\rho}{\mathrm{d}R}\right)^2 + \left(\frac{\mathrm{d}\eta}{\mathrm{d}R}\right)^2} \qquad \lambda_2 = \frac{\rho}{R}, \tag{1}$$

where the index 1 refers to meridians and 2 to parallels in the current configuration.

In the membrane approximation, it is assumed the deformation is normal preserving. Therefore the gradient of deformation admits the diagonal representation $\mathbf{F} = \mathrm{diag}(\lambda_1, \lambda_2, \lambda_3)$ in a local basis, where the eigenvalue λ_3 is relative to the membrane normal direction. By introducing the volumetric variation coefficient $J = \det \mathbf{F}$, we may therefore write

$$\lambda_3 = \frac{J}{\lambda_1 \lambda_2}. \tag{2}$$

With $\mathbf{F}$ written this way, we may now compute the 2D membrane energy from any 3D energy. Specifically here, to model the compressible behavior of the membrane, we use the three-dimensional Blatz–Ko strain energy density [97,98],

$$W^{3\mathrm{D}} = \alpha \frac{\mu}{2}\left[I_1 - 3 + \frac{1-2\nu}{\nu}\left(I_3^{-\frac{\nu}{1-2\nu}} - 1\right)\right] + (1-\alpha)\frac{\mu}{2}\left[\frac{I_2}{I_3} - 3 + \frac{1-2\nu}{\nu}\left(I_3^{\frac{\nu}{1-2\nu}} - 1\right)\right], \tag{3}$$

where $I_1 = \mathrm{tr}(\mathbf{F}\mathbf{F}^T)$, $I_3 = J^2$, $I_2 = I_3 \mathrm{tr}(\mathbf{F}\mathbf{F}^T)^{-1}$, and $0 < \alpha < 1$, $\mu > 0$, $-1 < \nu \leq 1/2$ are material constants. The infinitesimal shear modulus μ and infinitesimal Poisson ratio ν are related through $\mu = E/2(1+\nu)$, where E is the infinitesimal Young modulus. From hereon, it is understood that both E and ν are functions of R in the case of axisymmetric circular membranes: $E \equiv E(R)$ and $\nu \equiv \nu(R)$.

With the help of the plane-stress state condition [99,100], $P_{33}^{3\mathrm{D}} = 0$, where $\mathbf{P}^{3\mathrm{D}} = \partial W^{3\mathrm{D}}/\partial \mathbf{F}$ is the first Piola–Kirchhoff stress, we find the out-of-plane principal stretch ratio λ_3 as

$$\lambda_3 = \left(\lambda_1 \lambda_2\right)^{-\frac{\nu}{1-\nu}} = \Lambda^{\frac{1}{2}}, \qquad \text{where} \qquad \Lambda = \left(\lambda_1 \lambda_2\right)^{-\frac{2\nu}{1-\nu}}. \tag{4}$$

Now, by substituting Eq. (4) in Eq. (3), we obtain W, i.e. the *membrane strain energy function*, in terms of the two in-plane principal stretch ratios λ_1 and λ_2, as follows

$$W = E\frac{\alpha\left(\lambda_1^2 + \lambda_2^2\right) + (1-\alpha)\left(\lambda_1^{-2} + \lambda_2^{-2}\right) - 1}{4(1+\nu)} + E\frac{\left((\alpha-1)\Lambda^{-1} - \alpha\Lambda\right)(\nu-1) - 1}{4\nu(1+\nu)}. \tag{5}$$

Using Eq. (5), we then compute the non-zero components of the first Piola–Kirchhoff stress $\mathbf{P} = \partial W/\partial \mathbf{F}$ in the membrane as

$$P_i = \frac{\partial W}{\partial \lambda_i} = E\frac{\Lambda^{-1}\left(\lambda_i^2 - \Lambda\right)\left(1 + \alpha\left(\lambda_i^2\Lambda - 1\right)\right)}{2\lambda_i^3\,(1+\nu)}, \qquad i = 1, 2, \tag{6}$$

and the components of the principal Cauchy stress $\mathbf{T} = J^{-1}\mathbf{P}\mathbf{F}^T$ associated with the membrane energy, as

$$T_i = E\frac{\Lambda^{-\frac{3}{2}}\left(\lambda_i^2 - \Lambda\right)\left(1 + \alpha\left(\lambda_i^2\Lambda - 1\right)\right)}{2\lambda_i^2\lambda_1\lambda_2\,(1+\nu)}, \qquad i = 1, 2. \tag{7}$$

$$W^\star = \begin{cases} W\left(\lambda_1, \lambda_2\right) & \text{if} \quad \lambda_1 \geq \lambda_1^\star\left(\lambda_2, \nu\right), \quad \lambda_2 \geq \lambda_2^\star\left(\lambda_1, \nu\right), & \textbf{Taut region with biaxial tension}, \\ W\left(\lambda_1, \lambda_2^\star\left(\lambda_1, \nu\right)\right) & \text{if} \quad \lambda_1 \geq 1, \quad \lambda_2 \leq \lambda_2^\star\left(\lambda_1, \nu\right), & \textbf{Wrinkled region with uniaxial tension}, \\ W\left(\lambda_1^\star\left(\lambda_2, \nu\right), \lambda_2\right) & \text{if} \quad \lambda_2 \geq 1, \quad \lambda_1 \leq \lambda_1^\star\left(\lambda_2, \nu\right), & \textbf{Wrinkled region with uniaxial tension}, \\ 0 & \text{if} \quad \lambda_1 \leq 1, \quad \lambda_2 \leq 1, & \textbf{Slack region with no tension}. \end{cases} \tag{8}$$

Box I.

Note that in axially symmetric membranes, the Cauchy stress has only in-plane components (T_1, T_2) representing the principal stresses along meridians and parallels, respectively. With stretches given by Eq. (1), these are functions of R only.

It is worth noting that the Cauchy stress components Eq. (7) satisfy the *Baker–Ericksen inequality* $(T_2 - T_1)(\lambda_2 - \lambda_1) > 0$ for all choices of the material parameters. This condition is fundamental to ensure that an inflated, elastically homogeneous spherical membrane in its reference configuration remains spherical for all values of applied pressure, see De Tommasi et al. [101] and De Tommasi et al. [102]. In this paper we demonstrate that an initially flat membrane with elastic inhomogeneities can attain non-trivial geometries (other than the spherical configuration) under a uniform pressure load. Furthermore, wrinkles and necks may be achieved at desired locations.

2.1. Tension field theory: Relaxed strain energy functional

Ideally, membranes with negligible bending stiffness may only achieve non-negative stress states as they cannot sustain in-plane compression. Real membranes, however, possess a small (albeit non-negligible) bending stiffness which effectively slightly delays the onset of wrinkling when compressive stresses arise.

Lack of resistance to compression may be seen as a unilateral constitutive constraint. This is embedded in tension field theory by constructing a "relaxed strain energy density" $W^\star(\lambda_1, \lambda_2)$ from the parent energy $W(\lambda_1, \lambda_2)$, which sets an in-plane stress component to zero whenever it would be negative in the parent energy. Clearly, in taut regions $W^\star \equiv W(\lambda_1, \lambda_2)$, whereas in completely slack regions $W^\star = 0$.

Following Pipkin [77], we may formalize the above by taking (see the Eq. (8) in Box I).

The function $\lambda_i^\star(\lambda_j, \nu)$ is called "natural width in tension" and is the main player of the relaxed energy construction. Now consider a strip of membrane with energy Eq. (5), oriented along the principal directions. If the membrane is pulled by so that $\lambda_1 \geq 1$ along the direction 1, while being free in the direction 2, the membrane contracts laterally with stretch ratio $\lambda_2 = \lambda_2^\star(\lambda_1, \nu)$. This value is found by solving $T_2(\lambda_1, \lambda_2) = 0$ for λ_2. Therefore if $\lambda_2 \leq \lambda_2^\star(\lambda_1, \nu)$, then $T_2 \leq 0$, and the membrane would be compressed in the non-relaxed energy. In tension field theory, this problem is avoided by assuming that if the membrane is compressed further than $\lambda_2^\star$, its energy does not change once $\lambda_2^\star$ is attained: namely, $W^\star(\lambda_1, \lambda_2) = W(\lambda_1, \lambda_2^\star(\lambda_1, \nu))$.

Physically, if λ_1 is kept fixed, there would be no energetic expenditure in shortening the membrane in the direction 2, below the natural width $\lambda_2^\star$. The same considerations apply to the perpendicular direction, whereas in the fully slack region, the energy is directly set to zero. For auxetic materials ($\nu < 0$), "lateral contraction" is changed to "lateral expansion", while all the remaining considerations are unchanged.

Remarkably, for membranes with energy defined by Eq. (5), the natural width depends on the Poisson ratio ν only, as follows,

$$\lambda_i^\star\left(\lambda_j, \nu\right) = \left(\lambda_j\right)^{-\nu}, \qquad i, j = 1, 2, \qquad i \neq j. \tag{9}$$

Note that for $\nu = 1/2$, we recover the expression for the natural width obtained in Steigmann and Pipkin [103] and Steigmann and Pipkin [79] for incompressible and isotropic membranes.

The dependence of the natural width in tension on the Poisson coefficient ν has not been explored much so far. However, this feature can be powerfully exploited to achieve non-trivial wrinkling patterns on demand. Indeed, as already illustrated by Venkata et al. [104] for stretched membranes, by carefully tuning the spatial distribution of E and ν, one can achieve unusual wrinkling patterns. This has a great potential in technological applications [105,106].

Auxetic materials have interesting properties: when $\lambda_1 > 1$, then $\lambda_2^\star > 1$, indicating that the membrane expands in all directions. This is a very strong difference between auxetic and classical membranes. Classical membranes always contract laterally when pulled in the perpendicular direction. In the next section, we discuss the implications of these features for both classical and auxetic functionally graded membranes.

2.2. Equilibrium of a pressurized membrane

Equilibrium equations of axially symmetric pressurized membranes are written along the meridian and normal directions [41,107,108]. If the reference membrane is flat, all involved fields depend on the reference radius R only, and the equilibrium equations take the form

$$T_1' + \frac{\rho'}{\rho}\left(T_1 - T_2\right) = 0, \qquad \kappa_1 T_1 + \kappa_2 T_2 = -P, \tag{10}$$

where $(\bullet)' = d/dR$ and the membrane curvatures κ_1 (curvature along a meridian line) and κ_2 (curvature along a parallel line) in axial symmetry may be calculated as

$$\begin{aligned} \kappa_1 &= \frac{\rho'\eta'' - \rho''\eta'}{\lambda_1^3} = \frac{(\lambda_2 R)'\lambda_1' - (\lambda_2 R)''\lambda_1}{\lambda_1^2\sqrt{\lambda_1^2 - \left((\lambda_2 R)'\right)^2}}, \\ \kappa_2 &= \frac{\eta'}{\rho\lambda_1} = -\frac{\mathbf{n}\cdot\mathbf{e}_r}{\rho} = -\frac{\sqrt{\lambda_1^2 - \left((\lambda_2 R)'\right)^2}}{\lambda_1\lambda_2 R}. \end{aligned} \tag{11}$$

Note that for κ_2 we have also used the alternative expression based on the outward normal $\mathbf{n}$ to the current surface, and on the radial unit vector $\mathbf{e}_r$ pointing outwards radially and perpendicularly to the membrane axis z. This expression exemplifies that the curvature of a parallel *does not coincide*, in general, with the curvature of the membrane along the parallel unless of course $\mathbf{n} \equiv \mathbf{e}_r$.

Because the membrane is flat in its reference configuration, the fields ρ, η must satisfy the following boundary conditions,

$$\rho(R_{\text{fin}}) = 0, \qquad \eta(R_{\text{fin}}) = 0. \tag{12}$$

Also, because point loads are not applied to the membrane, the suitable boundary conditions to be imposed on the functions ρ, η to avoid stretch and curvature singularities at the origin are

$$\lambda_1(0) = \lambda_2(0), \qquad \kappa_1(0) = \kappa_2(0). \tag{13}$$

Finally, to account for the presence of *wrinkling*, it is sufficient to write the equilibrium equations in terms of the relaxed counterparts $(T_1^\star, T_2^\star)$ as obtained from the relaxed energy through $\mathbf{T}^\star = J^{-1}(\partial W^\star/\partial\mathbf{F})\mathbf{F}^T$. This will automatically ensure that no compressive states can be achieved on the inflated membrane.

3. General insights into necks and wrinkles

Due to constitutive and geometric non-linearities, it would appear that little can be said in general on the placement of wrinkles and necks in an inflated membrane undergoing large deformations. Surprisingly, a careful analysis of the equilibrium equations of an inflated membrane, together with the implementation of tension field theory, provides a deep and fully general characterization of what type of instability patterns may or may not be expected in an inflated membrane.

Even more remarkably, these characterizations are *universal*, in the sense that they are independent of the choice of the (isotropic and elastic) constitutive behavior of the material. One such remarkable universal result is that *necks and wrinkles can never overlap*: this insight will be used in the sequel to produce alternating patterns of regions with wrinkling and necking.

In this section we collect these universal characterizations, calling them "*insights*", that apply to *all isotropic, axisymmetric and inflated membranes.* Their relevance to the present study is that one can use them as general guidelines to design the spatial distribution of elastic moduli to obtain desired patterns of wrinkles and necks in the inflated membrane. The insights also provide interesting characterizations of the membrane shape when wrinkles or necks occur, therefore helping to understand what type of shapes may, or may not, be obtained in an inflated membrane undergoing such instabilities.

As we deal with thin membranes that offer no resistance to compression, we use tension field theory and base our analysis on the equilibrium equations Eq. (10), expressed in terms of the relaxed Cauchy principal stress components $T_1^\star, T_2^\star$.

- **Insight 1:** *The membrane curvature along the parallels is always negative:* $\kappa_2 < 0$.
  First note that the equilibrium of a cap above a parallel can be written, in global form, by balancing pressure $P > 0$ and membrane tension, to give
  $$T_1^\star \kappa_2 + \frac{P}{2} = 0. \tag{14}$$
  Because, by definition, $T_1^\star \geq 0$, equilibrium imposes $T_1^\star > 0$ and $\kappa_2 < 0$ everywhere, which concludes the proof.
  In passing, note that $\kappa_2 = \eta'/(\rho\lambda_1)$ so that $\eta(R)$ is a decreasing function from $R = 0$ to $R = R_{\text{fin}}$. But $\eta(R_{\text{fin}}) = 0$, which means that $\eta(0) > \eta(R) > 0$, in agreement with the fact that a membrane inflated from below ($z < 0$) displaces upwards.
- **Insight 2:** *Wrinkles can never be aligned with parallels.*
  If such wrinkles were to occur it would result in $T_1^\star = 0$, but from Insight 1 we know this is not possible. Therefore, wrinkles can only be aligned with meridians.
- **Insight 3:** *The following inequality is always satisfied in the membrane:* $\kappa_1 \geq -2|\kappa_2|$.
  To prove this, we use Eqs. (10) and (14) to get[1]
  $$T_2^\star = -\frac{P}{\kappa_2}\left(1 - \frac{\kappa_1}{2\kappa_2}\right). \tag{15}$$
  Because $T_2^\star \geq 0$ and $\kappa_2 < 0$, and by setting $\kappa_2 = -|\kappa_2|$, we obtain
  $$\kappa_1 \geq -2|\kappa_2|. \tag{16}$$
  It can also be interpreted as $\kappa_1/\kappa_2 \leq 2$, always.
- **Insight 4:** *When wrinkles occur, the membrane curvatures are linked through:* $\kappa_1 = -2|\kappa_2|$.
  This result follows from the previous point with $T_2^\star = 0$.
- **Insight 5:** *Neck regions (where* $\kappa_G = \kappa_1\kappa_2 < 0$*) and wrinkled regions can never overlap.*
  If there is wrinkling, then $\kappa_1 = -2|\kappa_2| < 0$; therefore the Gaussian curvature becomes positive, $\kappa_G = \kappa_1\kappa_2 > 0$, and thus, no necking can occur in the region of wrinkling.
- **Insight 6:** *For necking to happen, the principal stresses must satisfy:* $T_2^\star \geq 2T_1^\star$.
  By using Eqs. (14) to (15), we obtain the principal curvatures in terms of stresses
  $$\kappa_1 = -\frac{P}{T_1^\star}\left(1 - \frac{T_2^\star}{2T_1^\star}\right), \qquad \kappa_2 = -\frac{P}{2T_1^\star},$$
  $$\kappa_G = \kappa_1\kappa_2 = \frac{P^2}{2T_1^{\star 2}}\left(1 - \frac{T_2^\star}{2T_1^\star}\right). \tag{17}$$
  For necking, we need $\kappa_G < 0$, and the result follows.[2]
  This insight may be also used to prove that wrinkles can never overlap necks. Indeed, for necks $2T_1^\star \leq T_2^\star$, for wrinkles $T_2^\star = 0$, and combining both we get $2T_1^\star \leq T_2^\star = 0$, which cannot occur because $T_1^\star$ must be strictly positive.
- **Insight 7:** *Neither wrinkling nor necking can take place at the apex of the membrane.*
  According to Eq. (13), both principal stretches are equal at the center of the membrane, i.e. $\lambda_1 = \lambda_2$ at $R = 0$. Therefore, we have $T_1^\star = T_2^\star$ and $\kappa_1 = \kappa_2$ at $R = 0$. Then, from Insights 4 and 6, we conclude that neither wrinkling nor necking can occur at the apex of the membrane.

Based on Insight 2, we conclude that slack regions and wrinkles aligned with parallels can never occur in the inflated membranes. These observations help us to simplify the relaxed energy function in Eq. (8) is given in Box I as follows,

$$W^\star = \begin{cases} W\left(\lambda_1, \lambda_2\right) & \text{if} \quad \lambda_1 \geq \lambda_1^\star\left(\lambda_2, \nu\right), \quad \lambda_2 \geq \lambda_2^\star\left(\lambda_1, \nu\right), \\ W\left(\lambda_1, \lambda_2^\star\left(\lambda_1, \nu\right)\right) & \text{if} \quad \lambda_1 \geq 1, \qquad\qquad \lambda_2 \leq \lambda_2^\star\left(\lambda_1, \nu\right). \end{cases} \tag{18}$$

We emphasize here that not all insights are directly helpful in providing guidance on how to design the functionally graded membrane to get desired instabilities. From Insights 1, 2, 3, 4, 5, and 7 we deduce important information on the shape of an inflated membrane, with remarkable bounds on the membrane curvatures in regions with and without instabilities. These insights dictate what shapes may be expected (or not expected) in an inflated membrane, regardless of its constitutive response.

From Insight 6, together with the consideration that $T_2^\star = 0$ leads to the appearance of wrinkles, we conclude that it is possible to create necks and wrinkles by tuning the ratio between $T_2^\star$ and $T_1^\star$. This method is used in the following sections to create instability patterns at desired locations.

4. Designing instabilities

In principle, it is logical to assume that the spatial distributions of the elastic moduli $E(R)$, $\nu(R)$ may be tuned to achieve wrinkles and necks at given locations. However, in practice, the inverse problem is difficult to solve due to geometric and constitutive nonlinearities. Here, through a semi-analytical formulation, we show that in auxetic membranes with elastic inhomogeneities, wrinkles occur in soft regions

[1] Note sign difference with respect to Hill [109] and Machado et al. [42] due to different notations.

[2] Using this condition, we can design a membrane material with alternating regions of low and high Young's modulus to create alternating regions of necking and wrinkling under a uniform pressure load.

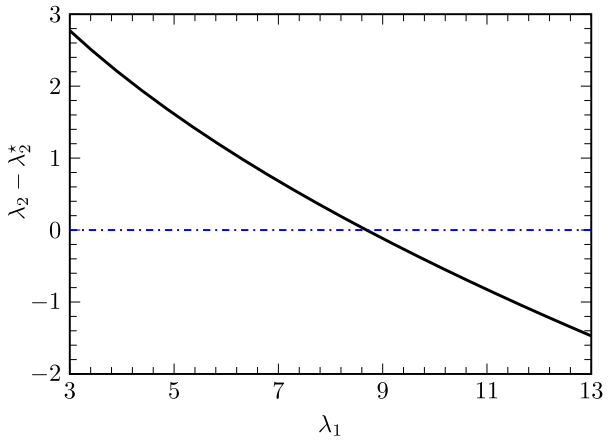

Fig. 3. Variation of $\lambda_2 - \lambda_2^\star$ with respect to λ_1. To simulate the behavior of this curve, any physically admissible arbitrary value of λ_2 can be chosen; here we take $\lambda_2 = 7$. For wrinkling to occur, we need $\lambda_2 - \lambda_2^\star \leq 0$, which is equivalent to the natural width condition, see Eq. (9).

(where E is low) and do not occur in stiff regions (where E is high), when there are no external boundary effects.

We recall that $T_1 > 0$ always, which results in the relaxed principal stress along the meridian $T_1^\star$ being strictly positive and continuous across the boundary between stiff and soft regions. As we do not consider rupture, λ_2 and the deformed radial component ρ are also continuous. Hence, across a boundary of radius R between elastically inhomogeneous regions, the following jump conditions apply for a physically valid solution,

$$[\![T_1^\star]\!] = 0, \qquad [\![\lambda_2]\!] = 0, \tag{19}$$

where $[\![f]\!] := \lim_{\epsilon\to 0}(f(R+\epsilon) - f(R-\epsilon))$. We see that across such a boundary, we may have a sharp jump in the tension $[\![T_2^\star]\!]$ along the parallels, while the value of $T_1^\star$ along the meridians remains continuous across the boundary. As a result of the continuity conditions in Eq. (19), we need $T_2 \leq 0$ (and therefore $T_2^\star = 0$) to produce wrinkles. From Eq. (7), we observe that $T_2 \leq 0$ implies $\lambda_2^2 - \Lambda \leq 0$, as all the other terms $(\Lambda, 1+\nu, 1-\alpha+\alpha\lambda_2^2\Lambda)$ are strictly positive. Therefore, for wrinkles to occur, it must result $\lambda_2 - \lambda_2^\star \leq 0$, where we made use of Eq. (4).

Let us now consider a phase boundary Γ between a wrinkled region and a non-wrinkled region. From Eq. (19) we know that λ_2 must be continuous over Γ and due to auxetic behavior $-\nu/1-\nu > 0$, therefore, Fig. 3 demonstrates that $\lambda_2 - \lambda_2^\star$ is a decreasing function of λ_1: Implying that when we move from a non-wrinkled region (where $\lambda_2 - \lambda_2^\star > 0$) to a wrinkled region (where $\lambda_2 - \lambda_2^\star < 0$), the meridian stretch λ_1 must increase.

But since we know from Eq. (19) that T_1 must be continuous across the phase boundary, this implies that the Young modulus E should decrease as one moves from a non-wrinkled region to a wrinkled region. Although this reasoning is certainly altered in the presence of boundary effects, we deduce from continuity considerations that wrinkling can be achieved by playing on the elastic stiffness contrast between neighboring regions. Specifically, to obtain wrinkles on the membrane, we can create patches of softer (low E) and stiffer (high E) regions, and wrinkles will occur in the softer regions, where the sudden increase of λ_1 will make $\lambda_2 - \lambda_2^\star$ negative.

This observation is corroborated by a numerical example, described in Fig. 4. We consider the inflation of a prestretched ($\lambda_p = 2$) circular membrane, fixed along its edge. The membrane is designed to have annular regions with high contrast of the Young modulus. Then, we find that upon inflation, wrinkles form only in soft regions (regions with low Young's modulus), confirming our predictions that wrinkles are generated when moving from a stiff towards a soft region.

Similarly, by tuning the ratio $E_{\text{stiff}}/E_{\text{soft}}$ between the Young modulus of two neighboring regions (now called "stiff" and "soft"), we can act on the ratio $T_2^\star/T_1^\star$ which, as the insights above reveal, regulates the onset of wrinkles (when $T_2^\star/T_1^\star$ is decreased toward 0) or the onset of necks (when $T_2^\star/T_1^\star$ is increased above 2).

The Poisson ratio ν is also a key player. Hence, when this coefficient is negative, the membrane expands laterally and creates compressive stresses ($T_2^\star = 0$).

The complexity of the problem requires a trial and error approach to determine appropriate elastic inhomogeneity patterns to achieve the sought instabilities. By using the commercial software COMSOL, we implement the Blatz–Ko relaxed strain energy function, Eq. (8), for functionally-graded, inflated membranes.

In the simulations, we inflate pre-stretched membranes by keeping the external rim fixed. Then we solve Eq. (10) to obtain the Pressure–Volume (P–V) curves (see the next section) and the deformation profiles of the membranes. The P–V plot is a global curve, and it cannot easily provide local information on some specific types of instabilities such as wrinkles. The softening or snap-through induced by necks is easily revealed in the P–V curve, because necks result in double-bubbling. This has been reported in experiments to be connected to a sudden jump in the volume. On the other hand, wrinkling, as we prove in general, can never induce double-bubbling. Therefore, there is no sudden variation in volume and qualitatively, we may expect that the effects of necks are more apparent in the P–V curve than the effects of wrinkles.

The numerical implementation is explained in Appendix A. Our simulations are consistent with the universal insights developed above: notably, we see that necking cannot occur in wrinkling regions and that only wrinkles aligned with meridians can occur. By playing on the ratio $E_{\text{stiff}}/E_{\text{soft}}$ and on the location of elastically inhomogeneous regions, we show that a desired number of wrinkling and necking regions can be obtained at prescribed locations.

For the sake of brevity, the effects of pre-stretch and of the Blatz–Ko material parameters are not discussed in detail. Here, we focus on the most relevant design parameters: ν and $E_{\text{stiff}}/E_{\text{soft}}$.

4.1. Necks and no wrinkles

To ensure that the inflated membrane develops necks without wrinkles, we have to create regions where the ratio $T_2^\star/T_1^\star$ exceeds 2, while maintaining $T_2^\star > 0$ everywhere in the membrane. To achieve this goal, in Section 4.1, we use a one-step variation of the Young modulus. The reference membrane has a central region with low Young's modulus (E_{soft}) surrounded by a region of high Young's modulus (E_{stiff}) which extends up to the boundary, as shown in Fig. 5. Moreover, to avoid that $T_2^\star$ approaches zero, we set $0 < \nu < -0.6$ which ensures a low-to-moderate auxeticity.

Our simulations show that if $E_{\text{stiff}}/E_{\text{soft}}$ is small (<1.5), the membrane displays a smooth necking during inflation. If $E_{\text{stiff}}/E_{\text{soft}}$ is moderate ($1.5 < E_{\text{stiff}}/E_{\text{soft}} < 3$), the necking region is more prominent.

On the left panel of Fig. 6, we plot the P-V profiles of pre-stretched circular membranes with different sizes of the E_{soft} region. From Case A to Case D, the radius or size of E_{soft} region increases (see Eq. (B.1b)). We observe that, as the size of the soft region increases, the value of the limit-point pressure P_{lim} decreases. This clearly occurs because the bigger the soft region, the smaller the effective Young modulus.

The deformation profile at the end of the inflation process is shown for each case on the right panel of Fig. 6. Notice that, by adjusting the size of the low Young modulus region, we can shift the boundary of the necking region. Therefore necks may be obtained at any desired location. Note that the simulations confirm that necking cannot occur at the tip of the membrane, in agreement with Insight 7.

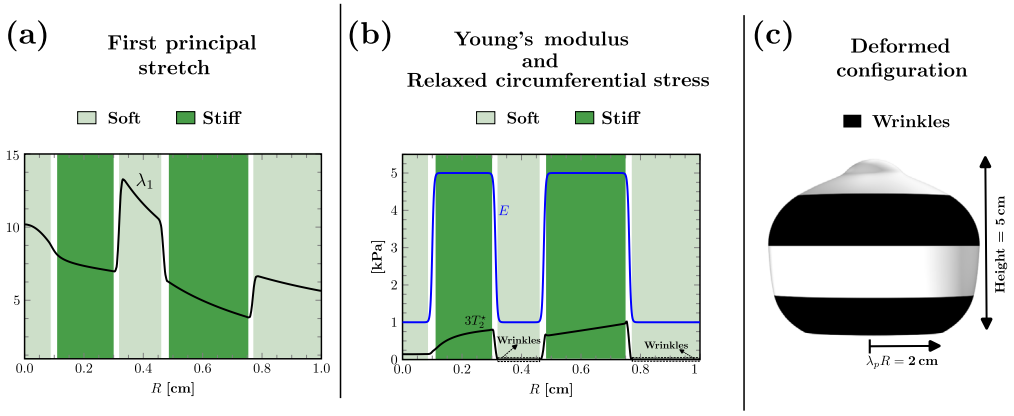

Fig. 4. Inflation of a prestretched ($\lambda_p = 2$) circular membrane fixed along its circumference. (a) Prescribed variation of the first principal stretch obtained using membrane strain energy function (Eq. (5)) with respect to the referential radial coordinate R. (b) Two-step variations of the Young modulus distribution and of three times the relaxed Cauchy stress along the parallels with R. (c) Corresponding deformed profile of the pressurized circular membrane with regions of wrinkles highlighted in black ($T_2^\star = 0$). We observe that wrinkles occur either in soft regions or in the region of the fixed boundary.

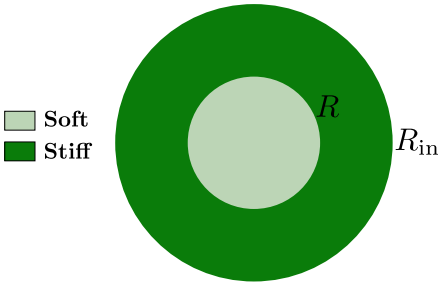

Fig. 5. Schematic representation of the one-step variation of the Young modulus distribution E in the reference configuration. The circular membrane has a softer region in the center surrounded by a stiffer region that extends to the disc circumference, see Eq. (B.1a).

Special case: Double bubbling

Membranes with a high stiffness ratio ($E_{\text{stiff}}/E_{\text{soft}} > 3$) undergo a transition into a *double-bubbled shape*, due to a sudden inflation of the softer region after the limit-point pressure, as shown in Fig. 7. In this figure, we plot the P–V curves for two different cases of one-step variation of the Young modulus.

It is important to note that the behavior of the P–V curve is strongly dependent on the size of the softer core. In Fig. 7(a), the volume decreases immediately after the limit point, whereas in Fig. 7(b) the volume keeps increasing while the pressure decreases after the limit point. Note that case (a) is also studied by Selvadurai [49] for pressurized incompressible elliptical membranes with the Ogden strain energy model.

We also show the deformed shapes at four different stages of inflation. Note that the formation of the second bubble corresponds to the necking point on the P–V curve.

Highly auxetic membranes (with $\nu < -0.8$) develop wrinkles in the region between the two bubbles. Indeed, high auxeticity results in high compressive stresses. Note that in line with Insight 5, wrinkles (black color regions) are never observed in the necking region, but only slightly above the neck.

4.2. Necks and wrinkles

In this section, we extend the findings from Section 4.1 to the general case where the Young modulus has an n-step variation across the membrane, while $\nu = -0.9$ is uniform throughout the membrane. Again, we use alternating stiff and soft regions to create multiple necks. Depending on the size of these regions we may or may not achieve lateral compression, and therefore wrinkling, in the membrane. Interestingly, the complexity of the problem leads to wrinkling regions appearing and disappearing during the inflation process.

The simulations show that membranes with n-step variations of the Young modulus develop $n - 1$ wrinkled regions during the pre-stretching process, consistent with the findings of Venkata et al. [104]. We recall that during pre-stretching, the membrane remains flat. These simulations are reported in Fig. 8, showing the onset of wrinkling patterns in laterally pre-stretched membranes with two- and three-step variations of the elastic moduli.

Following the pre-stretch, we simulate the inflation. The deformation profiles for the inflation process are shown in Fig. 9(b). Wrinkling and necking regions are represented by black (right half of the figure) and blue (left half) colors, respectively. Our simulations show that stiff regions inflate relatively less than soft regions. Moreover, this difference leads to the formation of a neck at the boundary between the two regions. Interestingly, the wrinkles generated during the pre-stretch phase tend to be preserved during the inflation process. Also, the wrinkles never overlap with the necking regions, which is consistent with the findings of Insight 5.

Furthermore, depending on the stiffness ratio between soft and stiff regions, the spacing between the necks and the wrinkles can be modulated. In particular, the higher the ratio $E_{\text{stiff}}/E_{\text{soft}}$, the closer the two patterns are, and vice-versa.

The spatial heterogeneity of the elastic moduli affects also the P–V curve, as shown in Fig. 9(a). Interestingly, for membranes with a two-step variation of the Young modulus, the pressure increases until the limit-point instability and later drops, whereas it remains nearly constant in the three-step variation case. In all simulations, no further increase of pressure past the limit point is observed, irrespective of the material constant $0 < \alpha < 1$.

Finally, we highlight two important features. First, configurations containing multiple regions of necks and wrinkles can be obtained by increasing the number of stiff-soft regions in the original membrane. Second, the pre-stretch λ_p may be used as a parameter to *unwrinkle*, during inflation, the regions of the membrane that are close to the boundary.

4.3. Wrinkles and no necks

Our results from the previous sections suggest that a high contrast between stiff and soft regions (i.e. high $E_{\text{stiff}}/E_{\text{soft}}$) leads to necking. Therefore, to avoid necks, we now consider a homogeneous (or nearly homogeneous) distribution of the Young modulus across the membrane. Although different types of distributions (constant, linear, step, and

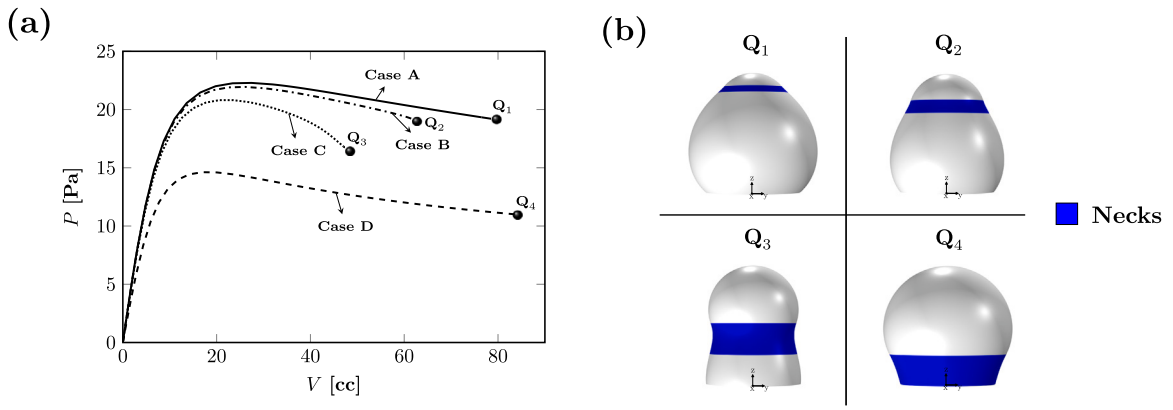

Fig. 6. (a) Inflation process: Pressure–Volume curves of a pre-stretched circular membrane with four different cases of one-step variation of the Young modulus. From Case A to Case D, the radius or size of E_{soft} region is assumed to be increasing (see Eq. (B.1b)), (b) Deformation profiles of the membrane at the end of inflation process are shown here for each case. The inflation process of each membrane is continued until the apex of the membrane reaches a height of five times the value of radius R_{in}. For each profile, the region in blue highlights the necking area ($\kappa_{\mathcal{G}} < 0$). Blatz–Ko parameter $\alpha = 0.4$, pre-stretch $\lambda_p = 2$, Poisson's ratio $\nu = -0.4$, and referential radius $R_{\text{in}} = 1$ cm.

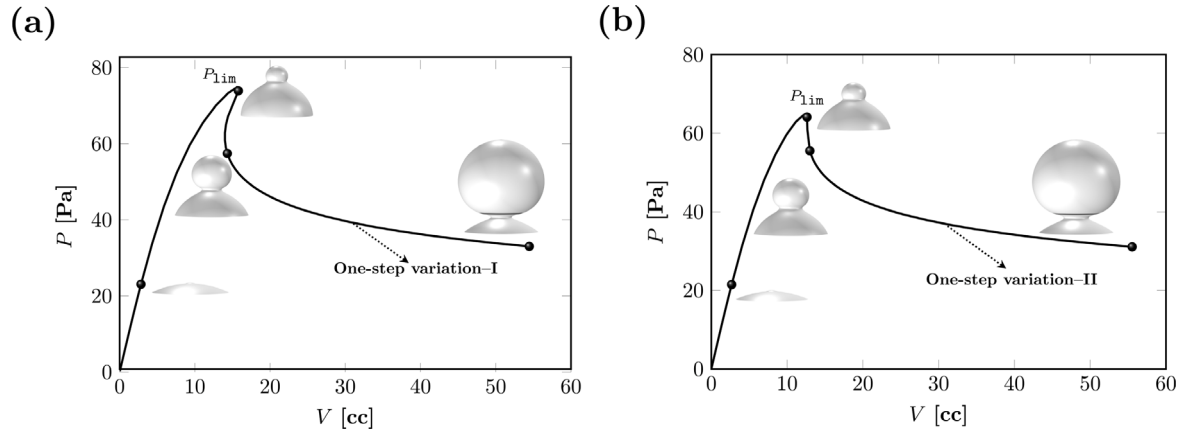

Fig. 7. Pressure–Volume curves of pre-stretched circular membranes for two different cases of one-step variation of the Young modulus (see, Eq. (B.1c)) are shown: (a) One-step variation–I, (b) One-step variation–II. The deformation profiles of the membrane are shown at four different points along the inflation path. The black region in the deformation profiles (at the end of the inflation process) denotes wrinkling regions. Parameters: $R_{\text{in}} = 1$ cm, $\lambda_p = 2$, $\alpha = 0.4$ and $\nu = -0.9$.

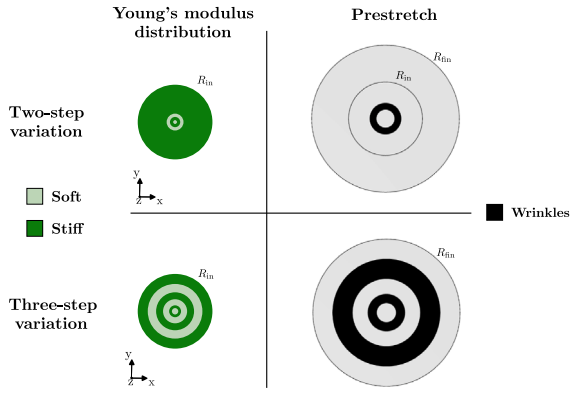

Fig. 8. First column: two-step (Eqs. (B.2a) to (B.2b)) and three-step (Eqs. (B.3a) to (B.3b)) variations in the Young modulus E. Right column: the corresponding wrinkling profiles appearing during the pre-stretch process. Here, the pre-stretch is $\lambda_p = 2$, with material parameters: $\alpha = 0.4$ and $\nu = -0.9$.

Gaussian) of the Poisson ratio are explored for this case, they all yield similar deformation behaviors.

For the sake of brevity, we consider the case where the material properties E, ν are spatially uniform throughout the membrane. We also compare our results with existing solutions in the literature.

In Fig. 10, we see that for an auxetic membrane with homogeneous Young's modulus, the pressure increases with the volume up to the limit point, where the membrane loses stability and wrinkles appear near the base of the membrane. Beyond the limit point, the pressure decreases with increasing volume. The results in Fig. 10 also show that the membrane attains a spherical shape, and indeed no necks are developed. These findings are consistent with previous experiments on pressurized incompressible circular membranes [38,42,110] and with several analytical and numerical studies [49,111,112].

For auxetic membranes, we predict the formation of wrinkles aligned with meridians. We note that Chaudhuri and DasGupta [92] predict wrinkles aligned with parallels in inflated incompressible membranes with homogeneous material properties. However, according to our Insight 2, such wrinkles are not possible in any axisymmetrically inflated isotropic circular membranes.

Additionally, we find that for a Blatz–Ko material with homogeneous material properties, tensile stresses exist everywhere in the membrane, except near the fixed circumferential edge. Hence, wrinkles are obtained only near the fixed boundary.

Finally, we mention that wrinkles, if present, may also be suppressed by tuning the Poisson ratio of the membrane and the pre-stretch applied to the membrane before inflating. We also observed separately that the limit-point pressure P_{lim} increases linearly with the Blatz–Ko material constant α and nonlinearly with the pre-stretch, respectively.

5. Conclusions

We demonstrated the possibility of harnessing various forms of instabilities such as wrinkling and necking using spatial material inhomogeneities in inflated hyperelastic auxetic membranes. In the finite

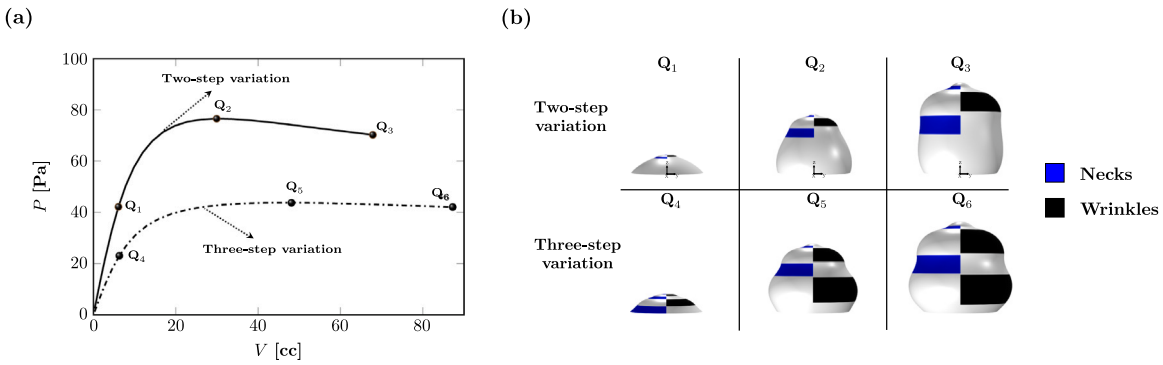

Fig. 9. (a) Inflation process: Pressure–Volume curves of a pre-stretched circular membrane with two-step (solid curve) and three-step (dash-dotted curve) variations of the Young modulus, (b) Deformation profiles of the membrane at three different locations are shown for each variation case. For each profile, the left half highlights the necking area in blue ($\kappa_{\mathcal{G}} < 0$) and the right half highlights the wrinkling area in black ($T_2^\star = 0$). Parameters: $\lambda_p = 2$, $\alpha = 0.4$ and $\nu = -0.9$.

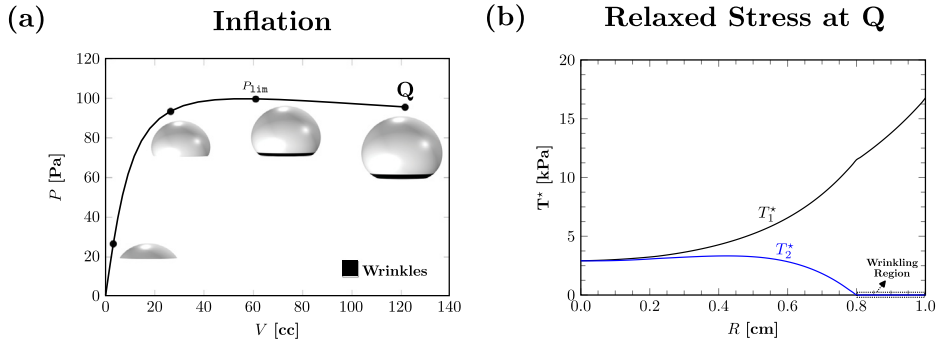

Fig. 10. (a) Pressure–Volume curve of pre-stretched circular membranes with constant material properties. The deformation profiles of the membrane are shown at four different points along the inflation path. The black region in the deformation profiles denotes wrinkling region, (b) Relaxed Cauchy stress along the meridians and parallels is denoted by $T_1^\star$ and $T_2^\star$, respectively. The wrinkling region corresponds to $T_2^\star = 0$. Parameters: $R_{\text{in}} = 1$ cm, $\lambda_p = 2$, $\alpha = 0.4$, $E = 70$ kPa, and $\nu = -0.9$.

element software (COMSOL), we implemented a relaxed strain energy function based on tension field theory to study the stability of an inflated compressible, hyperelastic membrane of the Blatz–Ko type for arbitrary geometry. Using an analytical formulation, we also derived a set of universal results for pressurized axisymmetric membranes. Finally, with inferences from universal results and through numerical simulations, we identified spatial inhomogeneity distributions across the undeformed membrane that result in wrinkles alone, necks alone, and simultaneous (but not overlapping) wrinkles and necks in the inflated membrane.

Our study is limited by various factors. For example, typical auxetic membranes are anisotropic in nature and their material properties are deformation-dependent: these features might greatly affect the results presented in this work. This aspect is not addressed in the current work but could be studied with the methods we have developed here. Another avenue of interest is to investigate the inflation of non-axisymmetric membranes. For example, in Fig. 11, we show 2D distributions of material properties in square membranes. The membrane is fixed on its edges and inflated under a uniform pressure load. We show that material properties can be tuned in the membranes to produce desired wrinkling patterns, as shown in Fig. 11. This concept could potentially be used in Braille reading and haptics.

CRediT authorship contribution statement

Sairam Pamulaparthi Venkata: Methodology, Software, Writing – original draft, Writing – review & editing. **Valentina Balbi:** Conceptualization, Writing – original draft, Writing – review & editing. **Michel Destrade:** Conceptualization, Writing – original draft, Writing – review & editing. **Giuseppe Zurlo:** Conceptualization, Methodology, Writing – original draft, Writing – review & editing.

Declaration of competing interest

On behalf of the co-Authors of this manuscript, I declare that we have no conflict of interest of any nature.

Data availability

No data was used for the research described in the article.

Acknowledgments

This project has received funding from the European Union's Horizon 2020 research and innovation programme under the Marie Skłodowska-Curie Grant Agreement No. 956401. GZ gratefully acknowledges the support of GNFM (Gruppo Nazionale di Fisica Matematica) of the INdAM F. Severi, Italy. The authors thank the anonymous referees for their valuable comments.

Appendix A. Numerical model in COMSOL

We adjust the pre-stretch λ_p by changing the radius of the undeformed membrane R_{in}, while holding the radius of the pre-stretched membrane R_{fin} fixed. Following [112,113], we represent the radial position of point $\mathcal{P}_2$ in the stretched membrane as

$$\rho_0 = \lambda_p R, \qquad \lambda_p = \frac{R_{\text{fin}}}{R_{\text{in}}}. \tag{A.1}$$

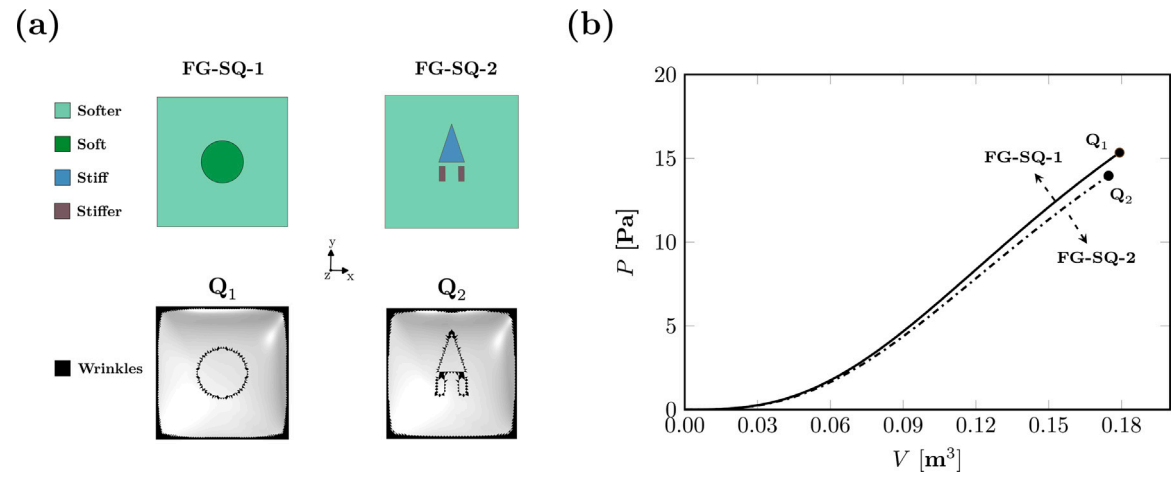

Fig. 11. (a) Square membranes with two different Young's modulus profiles (top) and wrinkling patterns (bottom); (b) Associated Pressure–Volume curves. FG-SQ-1: The circular region in the center and the rest of the membrane have $E = 0.3$ MPa and $E = 0.03$ MPa, respectively. FG-SQ-2: The triangular and rectangular strips have $E = 0.63$ MPa and $E = 4.03$ MPa, respectively, while the rest of the membrane has $E = 0.03$ MPa. The Poisson ratio is $\nu = -0.1$, pre-stretch $\lambda_p = 1$, and the Blatz–Ko coefficient is $\alpha = 0.4$. Wrinkling patterns at two points Q_1 and Q_2 on the inflation curves corresponding to FG-SQ-1 and FG-SQ-2, respectively, are shown at the bottom of (a).

We assume that the pre-stretched circular membrane is fixed on its boundaries, i.e. $\mathbf{u}(R_{\text{fin}}) = 0$, where $\mathbf{u}$ is the displacement field in the deformed membrane and R_{fin} is the radius of the pre-stretched circular membrane.

The initial thickness of the circular membrane is considered to be negligible in comparison to its radius (we take $H = R_{\text{in}}/200$). We take the Young modulus to vary spatially as a function of the referential radial coordinate R.

From an experimental viewpoint, the volume-controlled inflation process is performed by increasing the mass of the gas in the membrane [114]. However, in our simulations, we do not model the behavior of the gas. Instead, we implement the inflation by using a volume-controlled (or displacement-controlled) procedure as proposed by Yang and Feng [111], Pujara and Lardner [115], and Patil and DasGupta [112]. We prescribe a vertical displacement at the center of the membrane and calculate the corresponding pressure through a global optimization process using an inbuilt function in COMSOL.

The volume enclosed by the surface of the deformed membrane is computed as:

$$V = \frac{1}{3}\int_{\Omega} (\mathcal{Q}\cdot\mathbf{n})\,\mathrm{d}a, \tag{A.2}$$

where Ω represents the surface domain of the deformed membrane. The position vector of any point on the deformed surface of the membrane is represented by $\mathcal{Q}$ with $\mathbf{n}$ being the outward unit normal at that membrane point.

Here we briefly summarize the main features of that relaxed strain energy implementation in COMSOL software for axisymmetric circular membrane (see Venkata et al. [104]):

1. By taking advantage of axisymmetry around the Z-axis, we consider a line segment (which lies on mid-plane of the membrane) in (R, Z) plane with membrane elements for our analysis in a cylindrical coordinate system.
2. The relaxed energy functional (Eq. (8)) depends only on the principal stretches and material properties. In COMSOL, by using variable definitions under the component section in the model builder, we define mathematical expressions for the material properties. Principal stretches and invariants of the right Cauchy–Green tensor are then obtained by using internal variables in the software. Once the expressions for natural widths are defined, the relaxed strain energy functional is written in the definition window under the component section, which will be assigned as a user-defined hyperelastic model to the simulation geometry.
3. Once the boundary conditions and loading are assigned to the geometry with a desired mesh, different numerical solvers can be employed for the analysis.
4. In the post-processing stage, we obtain the location and orientation of wrinkles using logical operators based on the natural width conditions mentioned in Eq. (8).

Appendix B. Circular membranes

B.1. One-step variation in material properties

The variation in the Young modulus for the membrane is according to the following function:

$$E(R) = E_1 + E_2\left(\frac{\exp\{A\frac{(R-Y_1)}{D}\}-1}{\exp\{A\frac{(R-Y_1)}{D}\}+1}\right) - E_2\left(\frac{\exp\{A\frac{(R-Y_2)}{D}\}-1}{\exp\{A\frac{(R-Y_2)}{D}\}+1}\right). \tag{B.1a}$$

B.1.1. Only necks

$$\begin{aligned} &E_1 = 10\text{ kPa},\quad E_2 = 5\text{ kPa},\quad A = 2,\quad Y_2 = 1.1\text{ cm},\quad D = 0.003\text{ cm},\\ &Y_1 = 0.07875\text{ cm},\quad \text{(for Case A)},\quad Y_1 = 0.105\text{ cm},\quad \text{(for Case B)},\\ &Y_1 = 0.16125\text{ cm},\quad \text{(for Case C)},\quad Y_1 = 0.45\text{ cm},\quad \text{(for Case D)}, \end{aligned} \tag{B.1b}$$

B.1.2. Double bubbling

$$\begin{aligned} &E_1 = 10\text{ kPa},\quad E_2 = 30\text{ kPa},\quad A = 2,\quad Y_2 = 1.1\text{ cm},\quad D = 0.003\text{ cm},\\ &Y_1 = 0.115\text{ cm},\quad \text{(for one-step variation–I)},\\ &Y_1 = 0.145\text{ cm},\quad \text{(for one-step variation–II)}. \end{aligned} \tag{B.1c}$$

B.2. Multi-step variations in material properties: Interplay of necking and wrinkling behaviors

The two-step variation in the Young modulus for the membrane is expressed as

$$\begin{aligned} E(R) = E_1 &+ E_2\left(\frac{\exp\{A\frac{(R-Y_3)}{D_1}\}-1}{\exp\{A\frac{(R-Y_3)}{D_1}\}+1}\right) - E_2\left(\frac{\exp\{A\frac{(R-Y_4)}{D_1}\}-1}{\exp\{A\frac{(R-Y_4)}{D_1}\}+1}\right)\\ &+ E_2\left(\frac{\exp\{A\frac{(R-Y_5)}{D_1}\}-1}{\exp\{A\frac{(R-Y_5)}{D_1}\}+1}\right) - E_2\left(\frac{N_1\exp\{A\frac{(R-Y_6)}{D_1}\}-1}{\exp\{A\frac{(R-Y_6)}{D_1}\}+1}\right), \end{aligned} \tag{B.2a}$$

where

$$E_1 = 10 \text{ kPa}, \quad E_2 = 30 \text{ kPa}, \quad A = 2, \quad D_1 = 0.0085 \text{ cm}, \quad N_1 = 1.2,$$
$$Y_3 = 0.05 \text{ cm}, \; Y_4 = 0.1375 \text{ cm}, \; Y_5 = 0.225 \text{ cm}, \; Y_6 = 1.075 \text{ cm}. \tag{B.2b}$$

Similarly, the three-step variation in the Young modulus for the membrane is expressed as

$$\begin{aligned} E(R) = E_1 &+ E_2\left(\frac{\exp\{A\frac{(R-Y_7)}{D_2}\}-1}{\exp\{A\frac{(R-Y_7)}{D_2}\}+1}\right) - E_2\left(\frac{\exp\{A\frac{(R-Y_8)}{D_2}\}-1}{\exp\{A\frac{(R-Y_8)}{D_2}\}+1}\right) \\ &+ E_2\left(\frac{\exp\{A\frac{(R-Y_9)}{D_2}\}-1}{\exp\{A\frac{(R-Y_9)}{D_2}\}+1}\right) - E_2\left(\frac{\exp\{A\frac{(R-Y_{10})}{D_2}\}-1}{\exp\{A\frac{(R-Y_{10})}{D_2}\}+1}\right) \\ &+ E_2\left(\frac{\exp\{A\frac{(R-Y_{11})}{D_2}\}-1}{\exp\{A\frac{(R-Y_{11})}{D_2}\}+1}\right) - E_2\left(\frac{N_1\exp\{A\frac{(R-Y_{12})}{D_2}\}-1}{\exp\{A\frac{(R-Y_{12})}{D_2}\}+1}\right), \end{aligned} \tag{B.3a}$$

where

$$E_1 = 10 \text{ kPa}, \quad E_2 = 30 \text{ kPa}, \quad A = 2, \quad D_2 = 0.006 \text{ cm}, \quad N_1 = 1.2,$$
$$Y_7 = 0.085 \text{ cm},$$
$$Y_8 = 0.1625 \text{ cm}, \; Y_9 = 0.325 \text{ cm}, \; Y_{10} = 0.5125 \text{ cm}, \; Y_{11} = 0.7375 \text{ cm},$$
$$Y_{12} = 1.0375 \text{ cm}. \tag{B.3b}$$

Appendix C. Square membranes

C.1. Distribution of the Young modulus in the auxetic square membranes

The mathematical expression for the spatially varying Young's modulus of a quarter of the square membrane (FG-SQ-1) reads

$$\begin{aligned} E(X,Y) = &\mathcal{F}\left(\frac{L}{6} - X, \delta\right)\mathcal{F}\left(\sqrt{\left|\left(\frac{L}{6}\right)^2 - X^2\right|} - Y, \delta\right)E_1 \\ &+ \mathcal{F}\left(\frac{L}{2} - X, \delta\right)\mathcal{F}\left(\frac{L}{2} - Y, \delta\right)E_2, \end{aligned}$$
$$\text{where } \mathcal{F}(M,N) = 0.5 + 0.9375\left(\frac{M}{N}\right) - 0.625\left(\frac{M}{N}\right)^3 + 0.1875\left(\frac{M}{N}\right)^5,$$
$$\text{and } E_1 = 0.27 \text{ MPa}, \quad E_2 = 0.03 \text{ MPa}, \quad \delta = 10^{-20}, \quad L = 1 \text{ m},$$
$$0 \le X, Y \le \frac{L}{2}. \tag{C.1a}$$

Here, the left bottom vertex of the quarter square membrane is located at $(X = 0, Y = 0)$. The side length of the quarter square membrane in the undeformed configuration is $L/2$. The smoothed Heaviside function with a continuous second derivative is represented by $\mathcal{F}$, it is an inbuilt function in the COMSOL software. The function, $|(\bullet)|$, returns the absolute value of any variable, $(\bullet)$.

Similarly, for the full square membrane (FG-SQ-2) with side length L in the undeformed configuration, the Young modulus can be mathematically expressed as

$$\begin{aligned} E(X,Y) = &\mathcal{F}\left(X + \frac{2L_1}{3}, \delta\right)\mathcal{F}(\varepsilon - X, \delta)\mathcal{F}\left(3X + L_1 - Y, \delta\right) \\ &\times \mathcal{F}(Y + \varepsilon, \delta)E_1 \\ &+ \mathcal{F}\left(\frac{2L_1}{3} - X, \delta\right)\mathcal{F}(X - \varepsilon, \delta)\mathcal{F}\left(-3X + L_1 - Y, \delta\right) \\ &\times \mathcal{F}(Y + \varepsilon, \delta)E_1 \\ &+ \mathcal{F}\left(\frac{L}{2} - X, \delta\right)\mathcal{F}\left(\frac{L}{2} - Y, \delta\right)E_2 \\ &+ \mathcal{F}\left(X + \frac{L_1}{3}, \delta\right)\mathcal{F}\left(-\frac{L_1}{6} - X, \delta\right)\mathcal{F}\left(-\frac{2L_3}{3} - Y, \delta\right) \\ &\times \mathcal{F}\left(Y + L_2, \delta\right)E_3 \\ &+ \mathcal{F}\left(\frac{L_1}{3} - X, \delta\right)\mathcal{F}\left(X - \frac{L_1}{6}, \delta\right)\mathcal{F}\left(-\frac{2L_3}{3} - Y, \delta\right) \\ &\times \mathcal{F}\left(Y + L_2, \delta\right)E_3, \end{aligned}$$
$$E_1 = 0.6 \text{ MPa}, \; E_2 = 0.03 \text{ MPa}, \; E_3 = 4 \text{ MPa}, L = 1 \text{ m}, \; L_1 = \frac{2L}{7},$$
$$L_2 = \frac{L_1}{2},$$
$$L_3 = \frac{L_1}{7}, \; \delta = \varepsilon = 10^{-20}, \; -\frac{L}{2} \le X, Y \le \frac{L}{2}. \tag{C.1b}$$

References

[1] Popereka MY, Balagurov V. Ferromagnetic films having a negative Poisson ratio. Sov Phys Solid state 1970;11(12):2938–43.
[2] Milstein F, Huang K. Existence of a negative Poisson ratio in FCC crystals. Phys Rev B 1979;19(4):2030. http://dx.doi.org/10.1103/PhysRevB.19.2030.
[3] Lakes R. Foam structures with a negative Poisson's ratio. Science 1987;235(4792):1038–40. http://dx.doi.org/10.1126/science.235.4792.1038.
[4] Evans K, Caddock B. Microporous materials with negative Poisson's ratios. II. Mechanisms and interpretation. J Phys D: Appl Phys 1989;22(12):1883. http://dx.doi.org/10.1088/0022-3727/22/12/013.
[5] Milton GW. Composite materials with Poisson's ratios close to -1. J Mech Phys Solids 1992;40(5):1105–37. http://dx.doi.org/10.1016/0022-5096(92)90063-8.
[6] Love AEH. A treatise on the mathematical theory of elasticity. New York: Dover Publications I; 1944.
[7] Timoshenko S. History of strength of materials: with a brief account of the history of theory of elasticity and theory of structures. New York: Dover Publications; 1983.
[8] Wojciechowski K, Brańka A. Negative Poisson ratio in a two-dimensional "isotropic" solid. Phys Rev A 1989;40(12):7222. http://dx.doi.org/10.1103/physreva.40.7222.
[9] Ting TCT, Chen T. Poisson's ratio for anisotropic elastic materials can have no bounds. Quart J Mech Appl Math 2005;58(1):73–82. http://dx.doi.org/10.1093/qjmamj/hbh021.
[10] Frolich L, LaBarbera M, Stevens W. Poisson's ratio of a crossed fibre sheath: the skin of aquatic salamanders. J Zool 1994;232(2):231–52. http://dx.doi.org/10.1111/j.1469-7998.1994.tb01571.x.
[11] Bowick M, Cacciuto A, Thorleifsson G, Travesset A. Universal negative Poisson ratio of self-avoiding fixed-connectivity membranes. Phys Rev Lett 2001;87(14):148103. http://dx.doi.org/10.1103/PhysRevLett.87.148103.
[12] Lakes R. A broader view of membranes. Nature 2001;414(6863):503–4. http://dx.doi.org/10.1038/35107190.
[13] King WE, Anderson AT, Ferencz RM, Hodge NE, Kamath C, Khairallah SA, Rubenchik AM. Laser powder bed fusion additive manufacturing of metals; physics, computational, and materials challenges. Appl Phys Rev 2015;2(4):041304. http://dx.doi.org/10.1063/1.4937809.
[14] Sun S, Brandt M, Easton M. Powder bed fusion processes: An overview. Laser Addit Manuf 2017;55–77. http://dx.doi.org/10.1016/B978-0-08-100433-3.00002-6.
[15] Mueller S, Kruck B, Baudisch P. LaserOrigami: Laser-cutting 3D objects. In: Proceedings of the SIGCHI conference on human factors in computing systems. CHI '13, New York, NY, USA: Association for Computing Machinery; 2013, p. 2585–92. http://dx.doi.org/10.1145/2470654.2481358.
[16] Bhullar SK, Rana D, Lekesiz H, Bedeloglu AC, Ko J, Cho Y, Aytac Z, Uyar T, Jun M, Ramalingam M. Design and fabrication of auxetic PCL nanofiber membranes for biomedical applications. Mater Sci Eng: C 2017;81:334–40. http://dx.doi.org/10.1016/j.msec.2017.08.022.
[17] Lakes R. Advances in negative Poisson's ratio materials. Adv Mater 1993;5(4):293–6. http://dx.doi.org/10.1002/adma.19930050416.
[18] Bertoldi K, Vitelli V, Christensen J, Van Hecke M. Flexible mechanical metamaterials. Nat Rev Mater 2017;2(11):1–11. http://dx.doi.org/10.1038/natrevmats.2017.66.
[19] Ahmadi Bonakdar M, Chen XY, Sarbanha AA, Rodrigue D. Polybutylene succinate auxetic membrane produced by solution electrospinning. Adv Energy Mater 2023;25(21):2300699. http://dx.doi.org/10.1002/adem.202300699.
[20] Kolken HM, Janbaz S, Leeflang SM, Lietaert K, Weinans HH, Zadpoor AA. Rationally designed meta-implants: A combination of auxetic and conventional meta-biomaterials. Mater Horiz 2018;5(1):28–35. http://dx.doi.org/10.1039/C7MH00699C.

[21] Jiang H, Ziegler H, Zhang Z, Zhang H, Le Barbenchon L, Atre S, Chen Y. 3D printed tubular lattice metamaterials for mechanically robust stents. Composites B 2022;236:109809. http://dx.doi.org/10.1016/j.compositesb.2022.109809.

[22] Bonfanti A, Bhaskar A. Elastic stabilization of wrinkles in thin films by auxetic microstructure. Extreme Mech Lett 2019;33:100556. http://dx.doi.org/10.1016/j.eml.2019.100556.

[23] Chansoria P, Blackwell J, Etter EL, Bonacquisti EE, Jasiewicz N, Neal T, Kamal SA, Hoque J, Varghese S, Egan T, Nguyen J. Rationally designed anisotropic and auxetic hydrogel patches for adaptation to dynamic organs. Adv Funct Mater 2022;32(43):2207590. http://dx.doi.org/10.1002/adfm.202207590.

[24] Armstrong S, McHale G, Alderson A, Mandhani S, Meyari M, Wells GG, Carter E, Ledesma-Aguilar R, Semprebon C. Wetting transitions on superhydrophobic auxetic metamaterials. Appl Phys Lett 2023;123(15):151601. http://dx.doi.org/10.1063/5.0173464.

[25] Lazarus A, Reis PM. Soft actuation of structured cylinders through auxetic behavior. Adv Energy Mater 2015;17(6):815–20. http://dx.doi.org/10.1002/adem.201400433.

[26] Kaur M, Kim WS. Toward a smart compliant robotic gripper equipped with 3D-designed cellular fingers. Adv Intell Syst 2019;1(3):1900019. http://dx.doi.org/10.1002/aisy.201900019.

[27] Dolla WJS, Fricke BA, Becker BR. Structural and drug diffusion models of conventional and auxetic drug-eluting stents. J Med Devices 2006;1(1):47–55. http://dx.doi.org/10.1115/1.2355691.

[28] Gupta S, Gupta V, Chanda A. Biomechanical modeling of novel high expansion auxetic skin grafts. Int J Numer Methods Biomed Eng 2022;38(5):e3586. http://dx.doi.org/10.1002/cnm.3586.

[29] Beatty MF. Topics in finite elasticity: Hyperelasticity of rubber, elastomers, and biological tissues—With examples. Appl Mech Rev 1987;40(12):1699–734. http://dx.doi.org/10.1115/1.3149545.

[30] Evans SL. On the implementation of a wrinkling, hyperelastic membrane model for skin and other materials. Comput Methods Biomech Biomed Eng 2009;12(3):319–32. http://dx.doi.org/10.1080/10255840802546762.

[31] Fu B, Sperber E, Eke F. Solar sail technology—A state of the art review. Prog Aerosp Sci 2016;86:1–19. http://dx.doi.org/10.1016/j.paerosci.2016.07.001.

[32] Roddeman D, Drukker J, Oomens C, Janssen J. The wrinkling of thin membranes: Part I—Theory. 1987, http://dx.doi.org/10.1115/1.3173133.

[33] Cerda E, Ravi-Chandar K, Mahadevan L. Wrinkling of an elastic sheet under tension. Nature 2002;419(6907):579–80. http://dx.doi.org/10.1038/419579b.

[34] Amin F, Ali MN, Ansari U, Mir M, Minhas MA, Shahid W. Auxetic coronary stent endoprosthesis: Fabrication and structural analysis. J Appl Biomater Funct Mater 2015;13(2):127–35. http://dx.doi.org/10.5301/jabfm.5000213.

[35] Sun J, Gao H, Scarpa F, Lira C, Liu Y, Leng J. Active inflatable auxetic honeycomb structural concept for morphing wingtips. Smart Mater Struct 2014;23(12):125023. http://dx.doi.org/10.1088/0964-1726/23/12/125023.

[36] Bhullar SK, Lala NL, Ramkrishna S. Smart biomaterials-a review. Rev Adv Mater Sci 2015;40(3):303–14.

[37] Flint C, Naunton W. Physical testing of latex films. Rubber Chem Technol 1937;10(3):584–614. http://dx.doi.org/10.5254/1.3539012.

[38] Treloar L. Strains in an inflated rubber sheet, and the mechanism of bursting. Rubber Chem Technol 1944;17(4):957–67. http://dx.doi.org/10.5254/1.3546716.

[39] Rivlin RS, Saunders D. Large elastic deformations of isotropic materials VII. Experiments on the deformation of rubber. Philos Trans R Soc Lond Ser A 1951;243(865):251–88. http://dx.doi.org/10.1098/rsta.1951.0004.

[40] Adkins JE, Rivlin RS. Large elastic deformations of isotropic materials IX. The deformation of thin shells. Philos Trans R Soc Lond Ser A 1952;244(888):505–31. http://dx.doi.org/10.1098/rsta.1952.0013.

[41] Green AE, Adkins JE. Large elastic deformations and non-linear continuum mechanics. Oxford: Clarendon Press; 1960.

[42] Machado G, Favier D, Chagnon G. Membrane curvatures and stress-strain full fields of axisymmetric bulge tests from 3D-DIC measurements. Theory and validation on virtual and experimental results. Exp Mech 2012;52:865–80. http://dx.doi.org/10.1007/s11340-011-9571-3.

[43] Oden J, Sato T. Finite strains and displacements of elastic membranes by the finite element method. Int J Solids Struct 1967;3(4):471–88. http://dx.doi.org/10.1016/0020-7683(67)90002-9.

[44] Wriggers P, Taylor R. A fully non-linear axisymmetrical membrane element for rubber-like materials. Eng Comput 1990;7(4):303–10. http://dx.doi.org/10.1108/eb023817.

[45] Gruttmann F, Taylor R. Theory and finite element formulation of rubberlike membrane shells using principal stretches. Internat J Numer Methods Engrg 1992;35(5):1111–26. http://dx.doi.org/10.1002/NME.1620350511.

[46] Jiang L, Haddow J. A finite element formulation for finite static axisymmetric deformation of hyperelastic membranes. Comput Struct 1995;57(3):401–5. http://dx.doi.org/10.1016/0045-7949(94)00629-H.

[47] Rumpel T, Schweizerhof K, Haßler M. Efficient finite element modelling and simulation of gas and fluid supported membrane and shell structures. Text Compos Inflatable Struct 2005;153–72. http://dx.doi.org/10.1007/1-4020-3317-6_10.

[48] Eriksson A, Nordmark A. Instability of hyper-elastic balloon-shaped space membranes under pressure loads. Comput Methods Appl Mech Engrg 2012;237:118–29. http://dx.doi.org/10.1016/j.cma.2012.05.012.

[49] Selvadurai A. Mechanics of pressurized planar hyperelastic membranes. Phil Trans R Soc A 2022;380(2234):20210319. http://dx.doi.org/10.1098/rsta.2021.0319.

[50] Yang WH, Lu CH. General deformations of Neo-Hookean membranes. J Appl Mech 1973;40(1):7–12. http://dx.doi.org/10.1115/1.3422977.

[51] Adler A, Mikulas M. Application of a wrinkled membrane finite element approach to advanced membrane structures. In: AIAA space 2001 conference and exposition. 2001, p. 4646. http://dx.doi.org/10.2514/6.2001-4646.

[52] Lee E-S, Youn S-K. Finite element analysis of wrinkling membrane structures with large deformations. Finite Elem Anal Des 2006;42(8–9):780–91. http://dx.doi.org/10.1016/j.finel.2006.01.004.

[53] Barsotti R, Ligarò SS. Static response of elastic inflated wrinkled membranes. Comput Mech 2014;53:1001–13. http://dx.doi.org/10.1007/s00466-013-0945-5.

[54] Chen L, Nguyen-Thanh N, Nguyen-Xuan H, Rabczuk T, Bordas SPA, Limbert G. Explicit finite deformation analysis of isogeometric membranes. Comput Methods Appl Mech Engrg 2014;277:104–30. http://dx.doi.org/10.1016/j.cma.2014.04.015.

[55] Li M, Zhu K, Qi G, Kang Z, Luo Y. Wrinkled and wrinkle-free membranes. Internat J Engrg Sci 2021;167:103526. http://dx.doi.org/10.1016/j.ijengsci.2021.103526.

[56] Li M, Li Y, Zhang C, Qi G, Sui Y, Luo Y, Liu J. Stiffness modulation-driven wrinkle-free membrane. Appl Eng Sci 2022;9:100087. http://dx.doi.org/10.1016/j.apples.2022.100087.

[57] Fichter W. Some solutions for the large deflections of uniformly loaded circular membranes. Technical report, 1997.

[58] Coelho M, Roehl D, Bletzinger K-U. Numerical and analytical solutions with finite strains for circular inflated membranes considering pressure–volume coupling. Int J Mech Sci 2014;82:122–30. http://dx.doi.org/10.1016/j.ijmecsci.2014.03.012.

[59] Yuan J, Liu X, Xia H, Huang Y. Analytical solutions for inflation of pre-stretched elastomeric circular membranes under uniform pressure. Theor Appl Mech Lett 2021;11(3):100243. http://dx.doi.org/10.1016/j.taml.2021.100243.

[60] Foster HO. Inflation of a plane circular membrane. J Eng Ind 1967;89(3):403–7. http://dx.doi.org/10.1115/1.3610067.

[61] Yang X, Yu L, Long R. Contact mechanics of inflated circular membrane under large deformation: Analytical solutions. Int J Solids Struct 2021;233:111222. http://dx.doi.org/10.1016/j.ijsolstr.2021.111222.

[62] Pelliciari M, Sirotti S, Aloisio A, Tarantino AM. Analytical, numerical and experimental study of the finite inflation of circular membranes. Int J Mech Sci 2022;226:107383. http://dx.doi.org/10.1016/j.ijmecsci.2022.107383.

[63] Sirotti S, Pelliciari M, Aloisio A, Tarantino AM. Analytical pressure–deflection curves for the inflation of pre-stretched circular membranes. Eur J Mech A Solids 2023;97:104831. http://dx.doi.org/10.1016/j.euromechsol.2022.104831.

[64] Pelliciari M, Tarantino AM. A continuum model for circular graphene membranes under uniform lateral pressure. J Elasticity 2022;151(2):273–303. http://dx.doi.org/10.1007/s10659-022-09937-w.

[65] Haughton D, Ogden R. On the incremental equations in non-linear elasticity—I. Membrane theory. J Mech Phys Solids 1978;26(2):93–110. http://dx.doi.org/10.1016/0022-5096(78)90016-9.

[66] Haughton D, Ogden R. On the incremental equations in non-linear elasticity—II. bifurcation of pressurized spherical shells. J Mech Phys Solids 1978;26(2):111–38. http://dx.doi.org/10.1016/0022-5096(78)90017-0.

[67] Dym CL, Shames IH, et al. Solid mechanics. Springer; 1973, http://dx.doi.org/10.1007/978-1-4614-6034-3.

[68] Puntel E, Deseri L, Fried E. Wrinkling of a stretched thin sheet. J Elasticity 2011;105:137–70. http://dx.doi.org/10.1007/s10659-011-9340-7.

[69] Damil N, Potier-Ferry M. Influence of local wrinkling on membrane behaviour: a new approach by the technique of slowly variable Fourier coefficients. J Mech Phys Solids 2010;58(8):1139–53. http://dx.doi.org/10.1016/j.jmps.2010.04.002.

[70] Healey TJ, Li Q, Cheng R-B. Wrinkling behavior of highly stretched rectangular elastic films via parametric global bifurcation. J Nonlinear Sci 2013;23:777–805. http://dx.doi.org/10.1007/s00332-013-9168-3.

[71] Wang T, Yang Y, Fu C, Xu F. Competition between Mullins and curvature effects in the wrinkling of stretched soft shells. Int J Solids Struct 2022;241:111473. http://dx.doi.org/10.1016/j.ijsolstr.2022.111473.

[72] de Rooij R, Abdalla M. A finite element interior-point implementation of tension field theory. Comput Struct 2015;151:30–41. http://dx.doi.org/10.1016/j.compstruc.2015.01.007.

[73] Pagitz M, Abdalla M. Simulation of tension fields with in-plane rotational degrees of freedom. Comput Mech 2010;46(5):747–57. http://dx.doi.org/10.1007/s00466-010-0513-1.

[74] Pagitz M, Pellegrino S. Maximally stable lobed balloons. Int J Solids Struct 2010;47(11):1496–507. http://dx.doi.org/10.1016/j.ijsolstr.2010.02.013.

[75] Wagner H. Flat sheet metal girders with very thin metal web. Part I: General theories and assumptions. Technical report, 1931.

[76] Reissner E. On tension field theory. In: Proceedings of the fifth international congress for applied mechanics. Harvard University & MIT; 1938, p. 88–92.
[77] Pipkin AC. The relaxed energy density for isotropic elastic membranes. IMA J Appl Math 1986;36:85–99. http://dx.doi.org/10.1093/imamat/36.1.85.
[78] Pipkin A. Continuously distributed wrinkles in fabrics. Arch Ration Mech Anal 1986;95(2):93–115. http://dx.doi.org/10.1007/BF00281083.
[79] Steigmann DJ, Pipkin AC. Wrinkling of pressurized membranes. J Appl Mech 1989;56(3):624–8. http://dx.doi.org/10.1115/1.3176137.
[80] Steigmann D. Tension-field theory. Proc R Soc Lond Ser A Math Phys Eng Sci 1990;429(1876):141–73. http://dx.doi.org/10.1098/rspa.1990.0055.
[81] Pipkin AC. Relaxed energy densities for large deformations of membranes. IMA J Appl Math 1994;52(3):297–308. http://dx.doi.org/10.1093/imamat/52.3.297.
[82] Pipkin AC. Relaxed energy densities for anisotropic membranes. In: Parker DF, England AH, editors. IUTAM symposium on anisotropy, inhomogeneity and nonlinearity in solid mechanics. Dordrecht: Springer Netherlands; 1995, p. 333–8. http://dx.doi.org/10.1007/978-94-015-8494-4_45.
[83] De Tommasi D, Puglisi G, Zurlo G. Compression-induced failure of electroactive polymeric thin films. Appl Phys Lett 2011;98(12):123507. http://dx.doi.org/10.1063/1.3568885.
[84] De Tommasi D, Puglisi G, Zurlo G. Taut states of dielectric elastomer membranes. Int J Non-Linear Mech 2012;47(2):355–61. http://dx.doi.org/10.1016/j.ijnonlinmec.2011.08.002.
[85] Greaney P, Meere M, Zurlo G. The out-of-plane behaviour of dielectric membranes: Description of wrinkling and pull-in instabilities. J Mech Phys Solids 2019;122:84–97. http://dx.doi.org/10.1016/j.jmps.2018.09.006.
[86] Khurana A, Joglekar M, Zurlo G. Electromechanical stability of wrinkled dielectric elastomers. Int J Solids Struct 2022;246–247:111613. http://dx.doi.org/10.1016/j.ijsolstr.2022.111613.
[87] Khurana A, Kumar D, Sharma AK, Zurlo G, Joglekar M. Taut domains in transversely isotropic electro-magneto-active thin membranes. Int J Non-Linear Mech 2022;147:104228. http://dx.doi.org/10.1016/j.ijnonlinmec.2022.104228.
[88] Saxena P, Reddy NH, Pradhan SP. Magnetoelastic deformation of a circular membrane: Wrinkling and limit point instabilities. Int J Non-Linear Mech 2019;116:250–61. http://dx.doi.org/10.1016/j.ijnonlinmec.2019.07.006.
[89] Dhavale NN, Tamadapu G, DasGupta A. Finite inflation analysis of two circumferentially bonded hyperelastic circular flat membranes. J Appl Mech 2014;81(9):091012. http://dx.doi.org/10.1115/1.4027972.
[90] Barsotti R. Approximated solutions for axisymmetric wrinkled inflated membranes. J Appl Mech 2015;82(11):111007. http://dx.doi.org/10.1115/1.4031243.
[91] Pamulaparthi Venkata S, Saxena P. Instabilities in the free inflation of a nonlinear hyperelastic toroidal membrane. J Mech Mater Struct 2019;14(4):473–96. http://dx.doi.org/10.2140/jomms.2019.14.473.
[92] Chaudhuri A, DasGupta A. On the static and dynamic analysis of inflated hyperelastic circular membranes. J Mech Phys Solids 2014;64:302–15. http://dx.doi.org/10.1016/j.jmps.2013.11.013.
[93] Needleman A. Necking of pressurized spherical membranes. J Mech Phys Solids 1976;24(6):339–59. http://dx.doi.org/10.1016/0022-5096(76)90008-9.
[94] Chater E, Neale K. Finite plastic deformation of a circular membrane under hydrostatic pressure—II: Strain-rate effects. Int J Mech Sci 1983;25(4):235–44. http://dx.doi.org/10.1016/0020-7403(83)90027-9.
[95] Ulissi ZW, Govind Rajan A, Strano MS. Persistently auxetic materials: Engineering the Poisson ratio of 2D self-avoiding membranes under conditions of non-zero anisotropic strain. ACS Nano 2016;10(8):7542–9. http://dx.doi.org/10.1021/acsnano.6b02512.
[96] COMSOL multiphysics® version 6.0. Stockholm, Sweden: COMSOL AB; 2021, URL https://www.comsol.com/comsol-multiphysics.
[97] Blatz PJ, Ko WL. Application of finite elastic theory to the deformation of rubbery materials. Trans Soc Rheol 1962;6(1):223–52. http://dx.doi.org/10.1122/1.548937.
[98] Brockman RA. On the use of the Blatz-Ko constitutive model in nonlinear finite element analysis. Comput Struct 1986;24(4):607–11. http://dx.doi.org/10.1016/0045-7949(86)90199-9.
[99] Haughton D, McKay B. Wrinkling of annular discs subjected to radial displacements. Internat J Engrg Sci 1995;33(3):335–50. http://dx.doi.org/10.1016/0020-7225(94)00068-U.
[100] Haughton D, McKay B. Wrinkling of inflated elastic cylindrical membranes under flexure. Internat J Engrg Sci 1996;34(13):1531–50. http://dx.doi.org/10.1016/0020-7225(96)00059-6.
[101] De Tommasi D, Puglisi G, Zurlo G. A note on strong ellipticity in two-dimensional isotropic elasticity. J Elasticity 2012;109:67–74. http://dx.doi.org/10.1007/s10659-011-9370-1.
[102] De Tommasi D, Puglisi G, Zurlo G. Inhomogeneous spherical configurations of inflated membranes. Contin Mech Thermodyn 2013;25:197–206. http://dx.doi.org/10.1007/s00161-012-0240-2.
[103] Steigmann D, Pipkin A. Finite deformations of wrinkled membranes. Quart J Mech Appl Math 1989;42(3):427–40. http://dx.doi.org/10.1093/qjmam/42.3.427.
[104] Venkata SP, Balbi V, Destrade M, Accoto D, Zurlo G. Programmable wrinkling for functionally-graded auxetic circular membranes. Extreme Mech Lett 2023;63:102045. http://dx.doi.org/10.1016/j.eml.2023.102045.
[105] Naebe M, Shirvanimoghaddam K. Functionally graded materials: A review of fabrication and properties. Appl Mater Today 2016;5:223–45. http://dx.doi.org/10.1016/j.apmt.2016.10.001.
[106] Ren X, Das R, Tran P, Ngo TD, Xie YM. Auxetic metamaterials and structures: A review. Smart Mater Struct 2018;27(2):023001. http://dx.doi.org/10.1088/1361-665X/aaa61c.
[107] Gurtin ME, Ian Murdoch A. A continuum theory of elastic material surfaces. Arch Ration Mech Anal 1975;57:291–323. http://dx.doi.org/10.1007/BF00261375.
[108] Libai A, Simmonds JG. The nonlinear theory of elastic shells. second ed.. Cambridge University Press; 1998, http://dx.doi.org/10.1017/CBO9780511574511.
[109] Hill R. C. a theory of the plastic bulging of a metal diaphragm by lateral pressure. Lond Edinb Dublin Philos Mag J Sci 1950;41(322):1133–42. http://dx.doi.org/10.1080/14786445008561154.
[110] Zhou L, Wang S, Li L, Fu Y. An evaluation of the Gent and Gent-Gent material models using inflation of a plane membrane. Int J Mech Sci 2018;146:39–48. http://dx.doi.org/10.1016/j.ijmecsci.2018.07.035.
[111] Yang W, Feng W. On axisymmetrical deformations of nonlinear membranes. J Appl Mech 1970;37(4):1002–11. http://dx.doi.org/10.1115/1.3408651.
[112] Patil A, DasGupta A. Finite inflation of an initially stretched hyperelastic circular membrane. Eur J Mech A Solids 2013;41:28–36. http://dx.doi.org/10.1016/j.euromechsol.2013.02.007.
[113] Gonçalves PB, Soares RM, Pamplona D. Nonlinear vibrations of a radially stretched circular hyperelastic membrane. J Sound Vib 2009;327(1–2):231–48. http://dx.doi.org/10.1016/j.jsv.2009.06.023.
[114] Ericksen JL. Introduction to the thermodynamics of solids, Vol. 275, Springer; 1998.
[115] Pujara P, Lardner T. Deformations of elastic membranes—Effect of different constitutive relations. Z Angew Math Phys ZAMP 1978;29:315–27. http://dx.doi.org/10.1007/BF01601526.